LAWRENCE
LIVERMORE
NATIONAL
LABORATORY

LLNL-TR-664710

Neutronics Evaluation of Lithium-Based Ternary Alloys in IFE Blankets

A. Jolodosky, M. Fratoni

November 25, 2014

Disclaimer

This work performed under the auspices of the U.S. Department of Energy by Lawrence Livermore National Laboratory under Contract DE-AC52-07NA27344.

NEUTRONICS EVALUATION OF LITHIUM-BASED TERNARY ALLOYS IN IFE BLANKETS*

ALEJANDRA JOLODOSKY AND MASSIMILIANO FRATONI
UNIVERSITY OF CALIFORNIA, BERKELEY

FY 2014 REPORT

1 INTRODUCTION

Pre-conceptual fusion blanket designs require research and development to reflect important proposed changes in the design of essential systems, and the new challenges they impose on related fuel cycle systems. One attractive feature of using liquid lithium as the breeder and coolant is that it has very high tritium solubility and results in very low levels of tritium permeation throughout the facility infrastructure. However, lithium metal vigorously reacts with air and water and presents plant safety concerns. If the chemical reactivity of lithium could be overcome, the result would have a profound impact on fusion energy and associated safety basis. The overriding goal of this project is to develop a lithium-based alloy that maintains beneficial properties of lithium (e.g. high tritium breeding and solubility) while reducing overall flammability concerns. To minimize the number of alloy combinations that must be explored, only those alloys that meet certain nuclear performance metrics will be considered for subsequent thermodynamic study. The specific scope of this study is to evaluate the neutronics performance of lithium-based alloys in the blanket of an inertial confinement fusion (ICF) engine. The results of this study will inform the development of lithium alloys that would guarantee acceptable neutronics performance while mitigating the chemical reactivity issues of pure lithium.

2 MODELS AND METHODOLOGY

This analysis is based on a simplified model of an inertial fusion energy (IFE) chamber. Such model consists of a vacuum chamber of 1300.4 cm diameter with a point source at its center to represent the fusion process. The point source energy spectrum is shown in Figure 1. The energy spectrum is based on neutron scattering inside the lead capsule where the DT spherical source is located. The fusion chamber is enclosed by a series of layers made of structural material (HT9) or coolant as outlined in Table 1. A model of the entire system is illustrated in Figure 2. This model was reproduced in MCNP with ENDF/B-VII.1 cross sections at 900 K. Neutron transport simulations determined two main neutronics performance parameters for the blanket: tritium breeding ratio (TBR) that is the ratio of tritium produced in the system to tritium consumed, and the fusion energy multiplication factor (EMF) that is the ratio of power deposited in the blanket and other regions outside the LIFE chamber by neutrons, gammas, and alpha particles to the power derived from fusion. The EMF is defined in Equation (1):

$$EMF = \frac{total\ power}{fusion\ power} = \frac{E_d + E_\alpha}{17.6} \quad (1)$$

where E_d is the total energy deposited in the chamber (first wall, breeding regions, structures, and reflector) and surrounding regions (shield, beam dumps, etc.) as the result of neutron reactions, and E_α is the DT fusion alpha energy (3.5 MeV). The 17.6 in the denominator is the total energy in MeV released per fusion event. We include

*This work was performed under the auspices of the U.S. Department of Energy by Lawrence Livermore National Laboratory under Contract DE-AC52-07NA27344.

the neutron and neutron induced gamma energy deposited in regions outside the chamber with the expectation that this power will be recovered and contribute to the overall power cycle.

In this study it was required for the TBR to be greater than 1.02 in order for the system to be self-sufficient, including a 2% loss, and EMF to be greater than 1.10.

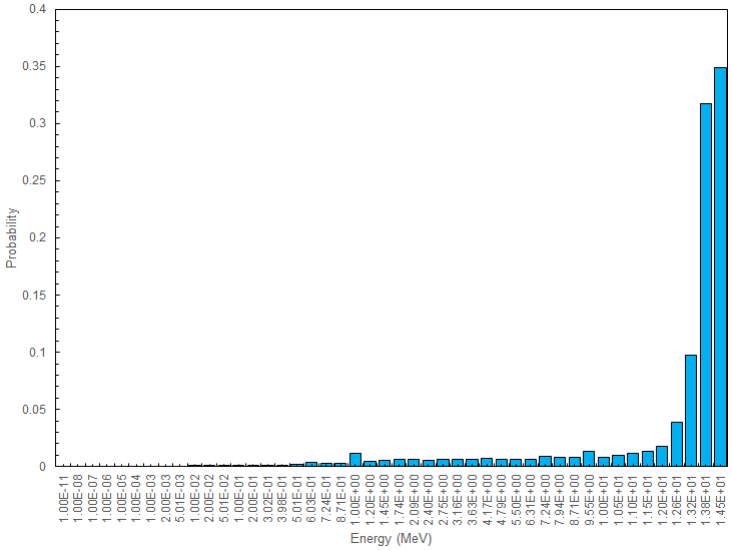

Figure 1: Fusion source neutron energy distribution.

Table 1: Composition and dimensions of the blanket components.

Layer, #	Material	Thickness, cm
1	HT9	0.5
2	Breeder/Coolant	1.0
3	HT9	0.5
4	Breeder/Coolant	100.0
5	HT9	0.5
6	Breeder/Coolant	50.0
7	HT9	0.5
8	Graphite	100.0

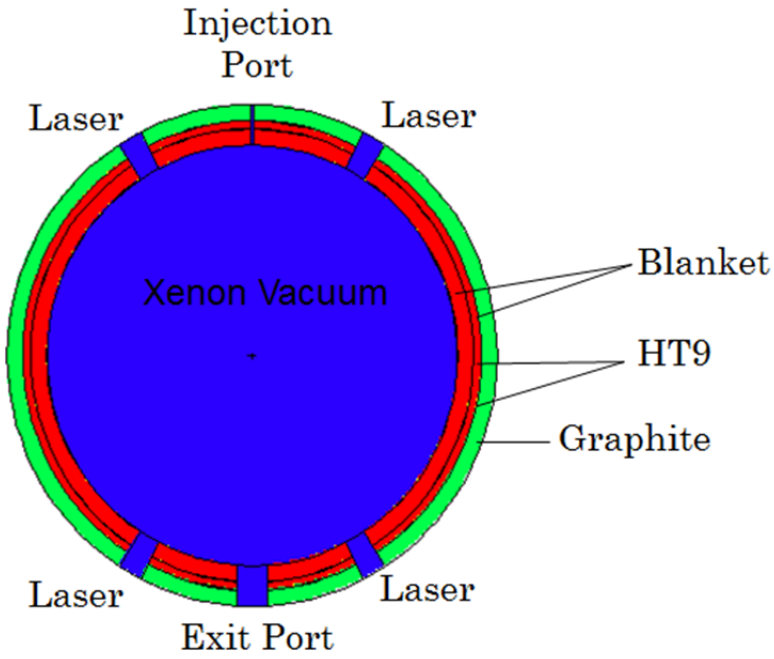

Figure 2: MCNP model of Life viewed from the xz plane.

3 RESULTS

3.1 BINARY ALLOYS

To better understand the neutronic behavior of lithium alloys we analyzed binary alloys. These can then be used to infer conclusions when combined in ternary systems. A subset of elements to analyze was provided by the Lawrence Livermore National Laboratory (LLNL) based on thermodynamics properties (sodium, magnesium, aluminum, silicon, calcium, titanium, copper, zinc, gallium, strontium, palladium, silver, indium, tin, antimony, barium, gold, lead, and bismuth). TBR and EMF for such binary alloys are illustrated in Figure 3. All values were calculated as function of lithium concentration in the alloy at 5% intervals. It is observed that:

1. Ba, Sn, and Ti offer the widest range of acceptable lithium concentration;
2. Bi and Pb do not meet the EMF requirement, but provide very large TBR even at low concentration of lithium, likely due to enhanced (n,xn) reactions;
3. Pd, In, and Ag feature a narrow acceptable range, but a relatively large EMF;
4. Sr, Ga, Cu, Na, Zn, Sb, and Au have very narrow or no acceptable compositions and limited EMF;
5. Mg, Al, Ca, and Si never meet both constraints, mainly due to their detrimental effect on EMF.

The lithium acceptable ranges for the binaries that meet constrains is summarized in Figure 4.

Table 2 provides effective properties for those the elements considered above. Effective neutron cross sections were calculated assuming a prototypical blanket neutron spectrum for a variety of reactions, i.e. (n,γ), (n,p), (n,d), (n,t), (n,He3), (n,α), (n,2n), and (n,3n). An effective Q-value was also calculated using equation (2):

$$Q_e = \frac{\sum_{i=1}^{N_e} x^i \sum_r Q_r^i \sigma_r^i}{\sum_{i=1}^{N_e} x^i \sum_r \sigma_r^i} \quad (2)$$

$$Q_{n,xn}^{i} = Q_{n,xn} + xQ_{e}^{Li} \quad (3)$$

where i is the specific isotope of an element, r is the type of neutron reaction, σ is the cross section, Q is the Q-value, x is the abundance fraction, and N_e is the number of isotopes in the element. The Q-value for (n,xn) reactions assumes that the additional neutrons will go on to be absorbed by lithium and is defined in (2). The x in equation (2) is either 2 or 3. From a neutronics perspective the following features are desirable:

- Low absorption cross section to reduce neutron loss[1];
- Large (n,xn) cross section to increase the number of neutrons in the blanket;
- High effective Q-value to enhance EMF.

The latest two are in contradiction as (n,xn) reactions are endothermic, but overall the availability of extra neutrons upon (n,xn) reaction may compensate the loss of energy due to subsequent exothermic reaction with ^{6}Li and/or other alloy constituents (e.g., lead and bismuth).

[1] We refer to absorption cross section as the sum of all cross sections for non-multiplying reactions.

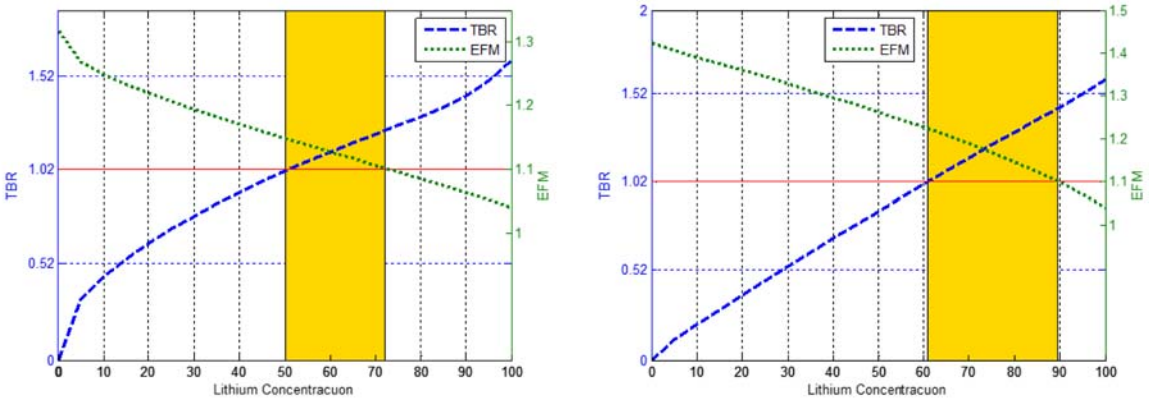

(a) LiBa

(b) LiSn

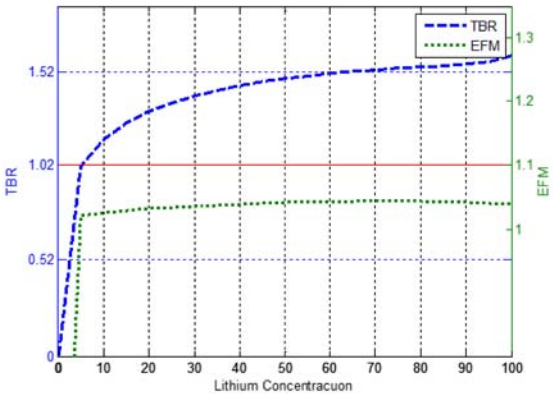

(c) LiBi

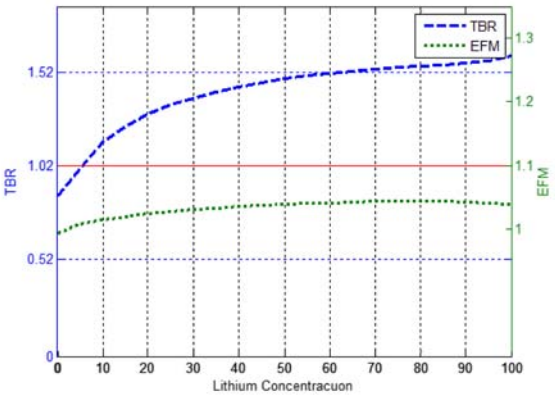

(d) LiPb

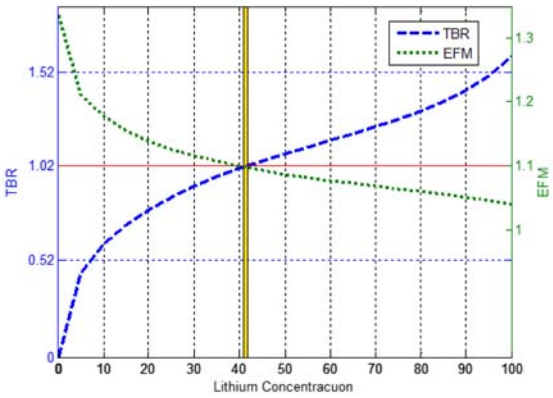

(e) LiSr

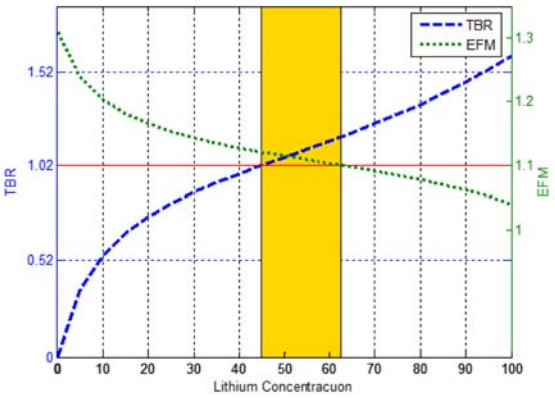

(f) LiTi

Figure 3: TBR and EMF for lithium binary alloys as a function of lithium concentration; the red line coincides with the minimum value for both TBR (1.02) and EMF (1.10), the shaded yellow area indicates the range of lithium concentration within which both constraints are met.

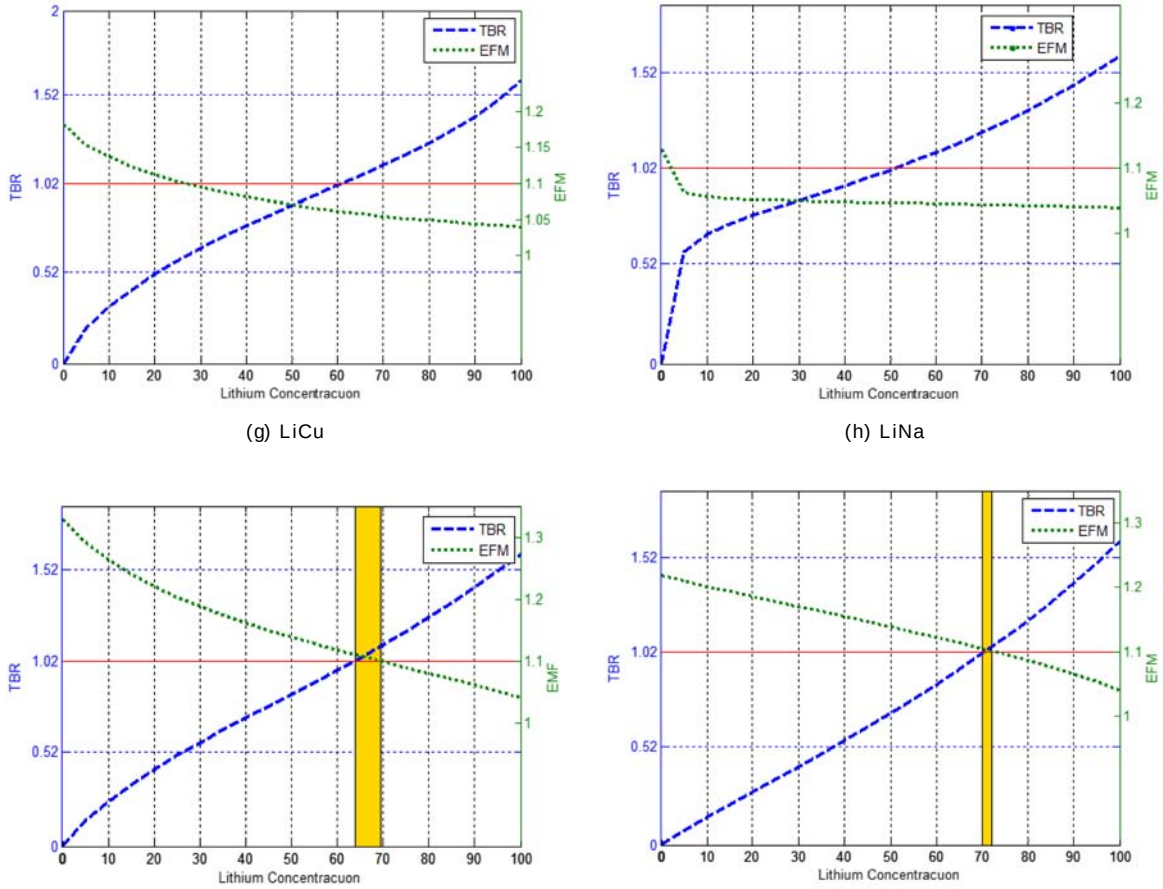

(g) LiCu (h) LiNa

(i) LiZn (j) LiGa

Figure 3: TBR and EMF for lithium binary alloys as a function of lithium concentration; the red line coincides with the minimum value for both TBR (1.02) and EMF (1.10), the shaded yellow area indicates the range of lithium concentration within which both constraints are met.

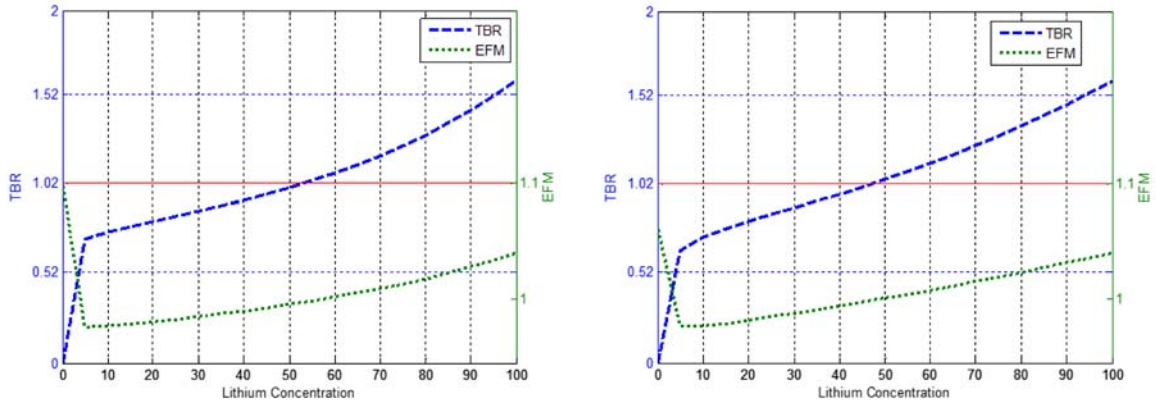

(k) LiMg (l) LiAl

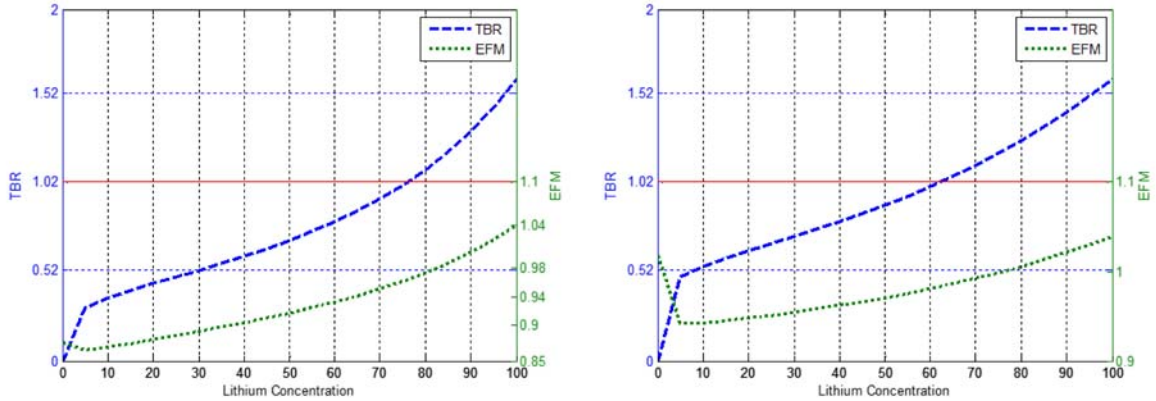

(m) LiCa (n) LiSi

Figure 3: TBR and EMF for lithium binary alloys as a function of lithium concentration; the red line coincides with the minimum value for both TBR (1.02) and EMF (1.10), the shaded yellow area indicates the range of lithium concentration within which both constraints are met.

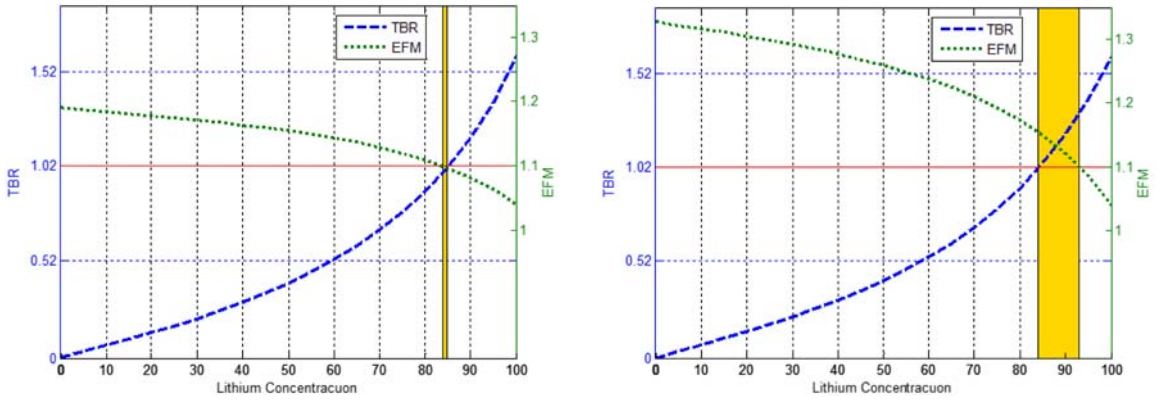

(o) LiSb

(p) LiPd

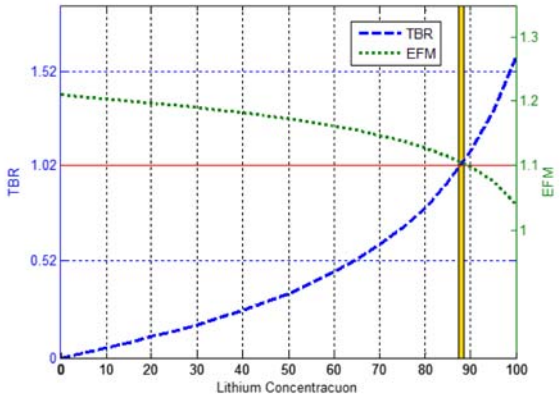

(q) LiAu

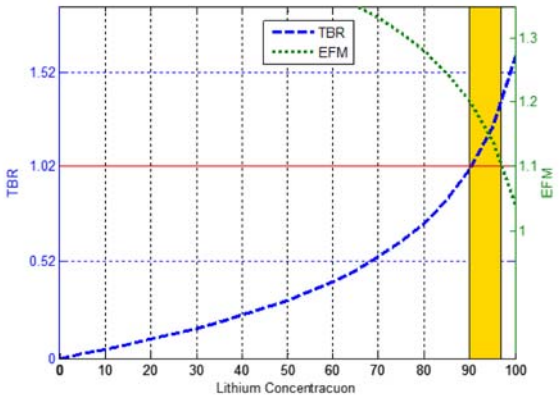

(r) LiAg

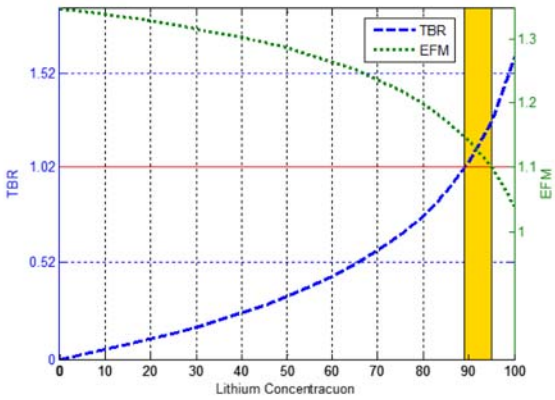

(s) LiIn

Figure 3: TBR and EMF for lithium binary alloys as a function of lithium concentration; the red line coincides with the minimum value for both TBR (1.02) and EMF (1.10), the shaded yellow area indicates the range of lithium concentration within which both constraints are met.

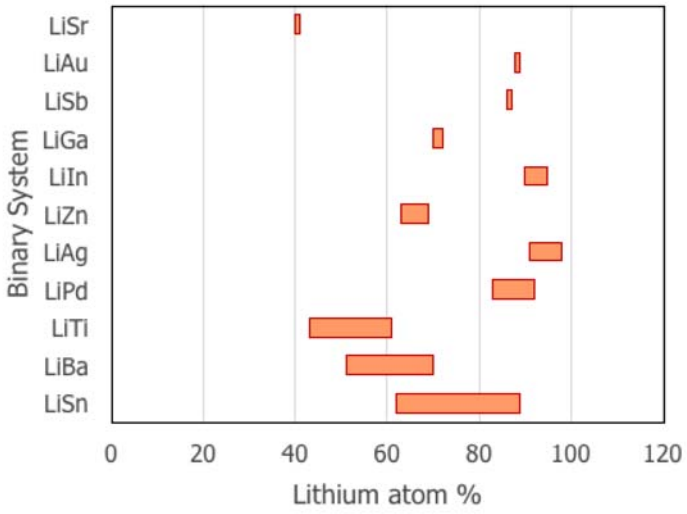

Figure 4: Summary of lithium ranges for binaries that meet TBR (1.02) and EMF (1.10) constrains.

Table 2: Effective cross sections and Q-values for selected elements.

Element	Q-value, MeV	Absorption	(n,xn) cross
Lithium	4.67	7.37E-02	1.53E-03
Lithium-6	4.78	9.77E-01	0.00E+00
Lithium-7	-7.16	4.63E-04	1.66E-03
Sodium	-1.79	1.53E-02	5.30E-04
Magnesium	-2.13	2.35E-02	4.77E-03
Aluminum	-0.96	1.57E-02	1.21E-04
Silicon	-2.67	3.21E-02	9.30E-04
Calcium	0.48	5.39E-02	5.31E-04
Titanium	3.47	2.78E-02	1.45E-02
Copper	5.12	7.24E-02	2.20E-02
Zinc	4.44	5.97E-02	1.24E-02
Gallium	5.45	1.33E-01	3.25E-02
Strontium	1.97	1.59E-02	3.11E-02
Palladium	6.86	3.72E-01	7.24E-02
Silver	6.37	6.50E-01	6.36E-02
Indium	6.20	6.68E-01	6.76E-02
Tin	4.18	7.51E-02	7.34E-02
Antimony	5.61	3.65E-01	6.82E-02
Barium	3.55	5.14E-02	7.99E-02
Gold	5.76	6.98E-01	1.07E-01
Lead	1.76	5.58E-03	1.17E-01
Bismuth	1.64	6.37E-03	1.14E-01

3.2 TERNARY ALLOYS

Similar analysis was conducted for ternary alloys in order to determine compositions that meet both TBR and EMF constraints. A total of 34 combinations were analyzed. TBR and EMF were calculated as a function of the alloy composition varying the amount of each element in the mixture from 0% to 100% by increments of 5%. Results were plotted in ternary graphs.

3.2.1 LiSnZn

Results for LiSnZn alloys are illustrated in Figure 5. The composition domain that fits both the TBR and EMF minimum values is shown in Figure 6. The concentration of lithium must remain between 61% and 88%. Incrementing tin or zinc concentration reduces TBR and increases EMF. Table 3 provides properties for some of the feasible limiting cases.

Among the acceptable cases, a composition of 70% lithium, 20% tin, and 10% zinc was chosen for further analysis. The neutron spectrum in different regions of the system is illustrated in Figure 7. A dip is observed in every region around 0.4 MeV. This is due to the resonance in the absorption cross section of lithium-6.

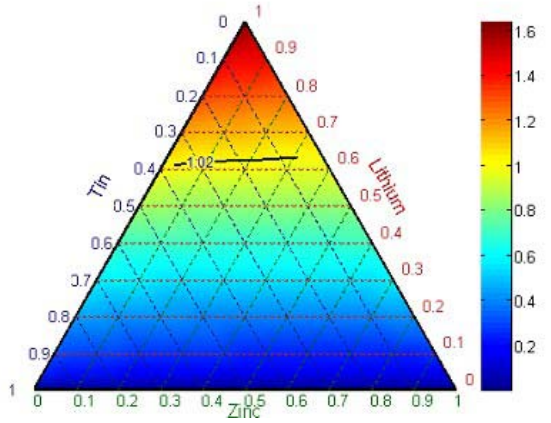

(a)

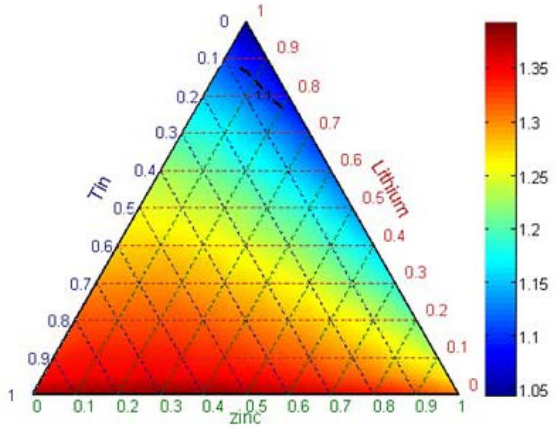

(b)

Figure 5: Tritium breeding ratio (a) and energy multiplication factor (b) for LiSnZn alloys as a function of composition.

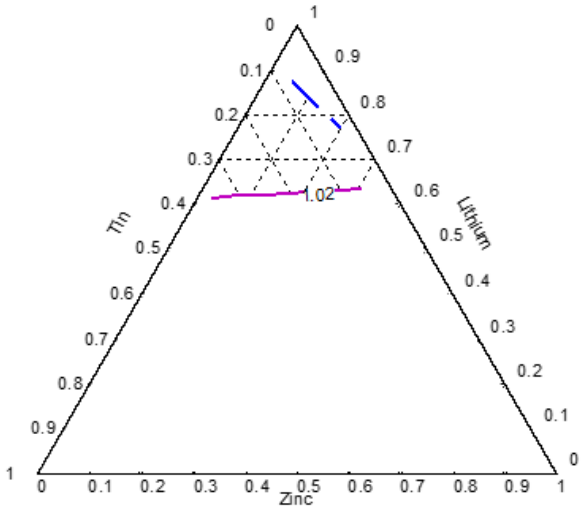

Figure 6: Acceptable domain of LiSnZn compositions.

Table 3: Properties of selected compositions within the acceptable domain for LiSnZn alloys.

Feature	Li, %	Sn, %	Zn, %	TBR	EMF
Min TBR, max EMF	61	36	3	1.02	1.22
Max TBR, min EMF	88	6	6	1.40	1.10
Reference	70	20	10	1.14	1.17
Min Li	61	36	3	1.02	1.22
Max Li	88	6	6	1.40	1.10
Max Sn	61	36	3	1.02	1.22

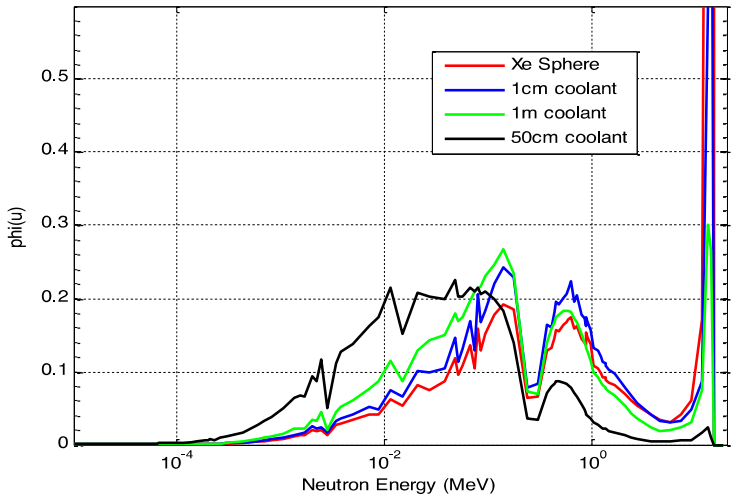

Figure 7: Neutron spectrum at different blanket positions for LiSnZn.

Figure 8 shows spatial resolution per until volume of the tritium reaction rate in a close-up the entire system, with the blanket layers numbered. The scale is arbitrary as its purpose is to visually illustrate where tritium production is maximized. As expected, the reaction rate is highest in the largest coolant region (layer 4) of the reactor and starts to decrease as it goes further out. What is notable is at the periphery where the graphite reflector is located, shown in Fig. 8 by the red line, the tritium reaction rate increases again. This is due to the back-scattered neutrons from the graphite reflector that features both a lower energy and increased probability of absorption in lithium-6, meaning tritium production. This phenomenon is illustrated in Figure 9 that compares neutron spectra in the layer adjacent to the reflector.

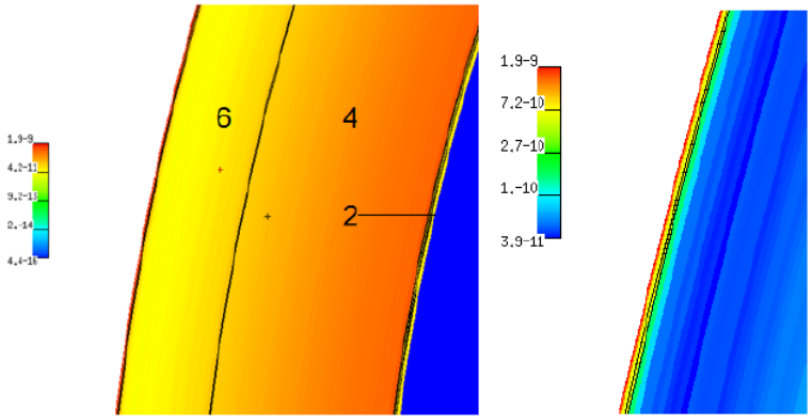

(a) (b)

Figure 8: Spatial resolution per unit volume of (n,t) reaction in (a) the xz direction for a close-up of the system with blanket layers labeled and (b) image zoomed showing increased (n,t) reaction at the periphery of reflector (arbitrary scale).

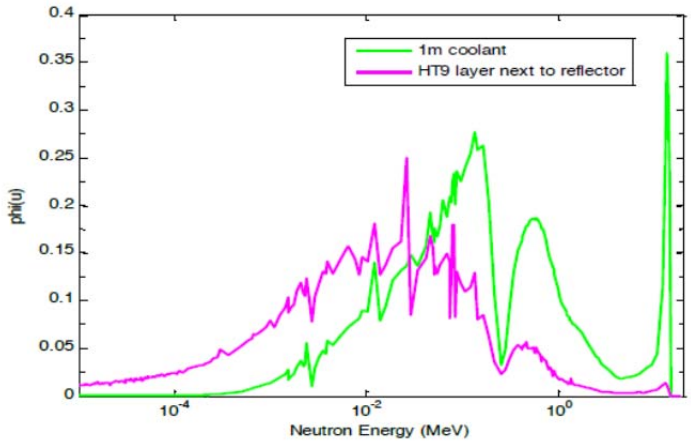

Figure 9: Comparison of neutron spectra between largest coolant layer and HT9 layer adjacent to reflector.

Table 4 gives a detailed breakdown of the contributions to the tritium breeding ratio by blanket region and type of reaction for the 70% Li, 20% Sn, 10% Zn case. As expected, the majority of the breeding occurs in the 100-cm-thick layer 4. On a per unit volume basis (last column of the table), the innermost layer is most effective due to the high energy reactions with ^{7}Li. In layer 6 (adjacent to the reflector) nearly all the tritium breeding is due to low energy neutron reactions with ^{6}Li.

Table 4: Contributions to TBR from ^{6}Li and ^{7}Li in the Three Breeder/Coolant Layers

Layer number	Volume (m^3)	Vol. Fraction (VF)	T6	T7	Layer TBR = T6+T7	TBR/VF
2	5.33	0.0053	0.01416	0.00815	0.02232	4.21050
4	620.68	0.6167	0.80540	0.21904	1.02444	1.66116
6	380.15	0.3778	0.09278	0.00237	0.09515	0.25184
Total	1006.15	1.0000	0.91234	0.22956	1.14190	1.14190

T6 = ^{6}Li(n,T) reactions per DT fusion
T7 = ^{7}Li(n,n'T) reactions per DT fusion

Assessment of neutron loss by (n,t) reaction in the thermal energy range (<0.1 MeV) and in the fast energy range (from 0.1 MeV to 20 MeV) is seen in Figure 10a. Higher reaction rates are seen in the thermal spectrum as expected for light elements with dominant $1/v$ cross section behavior. However, more energy is deposited by neutrons and photons at higher energies as outlined in Figure 10b. Because more neutrons are lost by (n,γ) reactions in the thermal range 10c, it is concluded that larger energy deposition in the fast spectrum is due to neutron absorption at higher energies. Future work will look at the option of optimizing the blanket performance modifying the neutron spectrum.

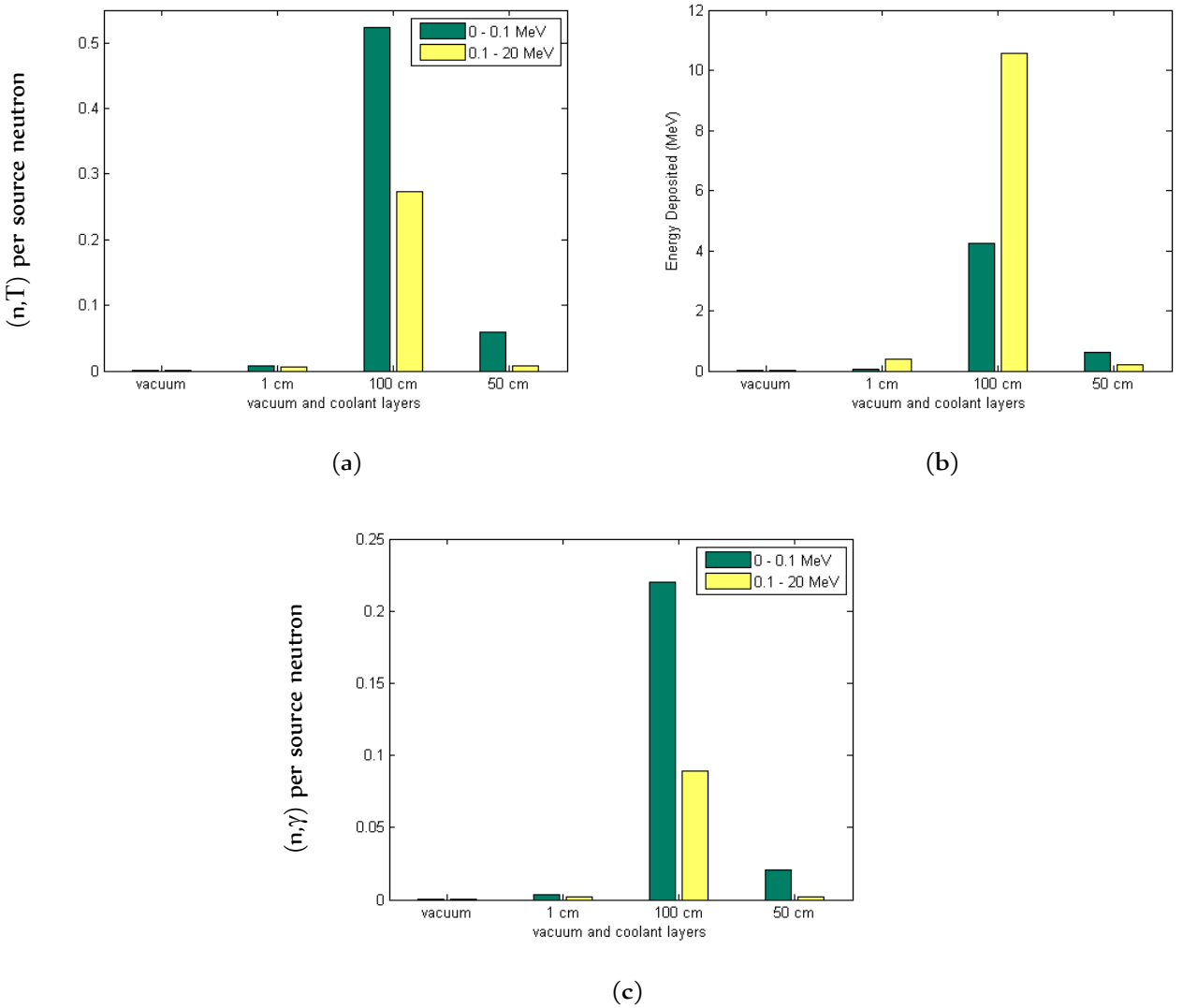

Figure 10: Comparison of thermal and fast spectra contributions for (a) tritium breeding reactions, (b) total energy deposition and (c) (n,γ) reactions

3.2.3 LiSnCa

Ternary plots of TBR and EMF for LiSnCa alloys are shown in Figure 11. In comparison to zinc, calcium produces a smaller EMF. Absorption reactions excluding (n,xn) are higher in calcium while (n,2n) reactions are smaller; this decreases the EMF. The TBR is slightly smaller than the zinc case. Since lithium is the major contributor of the TBR, results are similar in both instances. The resulting area that meets both design requirements (Figure 12) is considerably smaller. Data for limiting cases are provided in Table 5

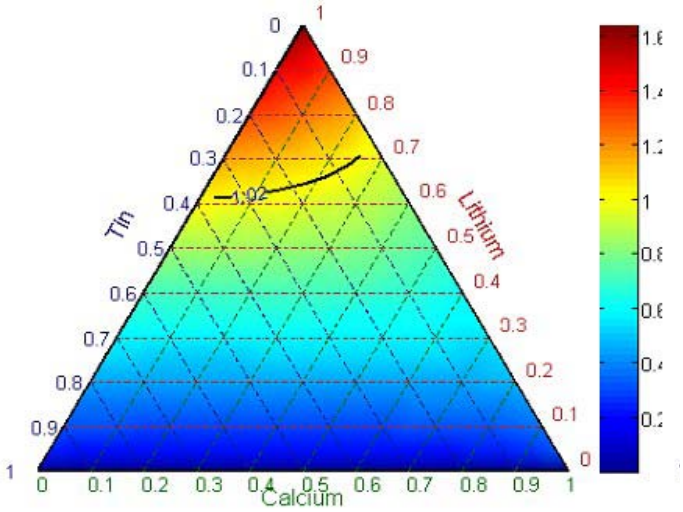

(a)

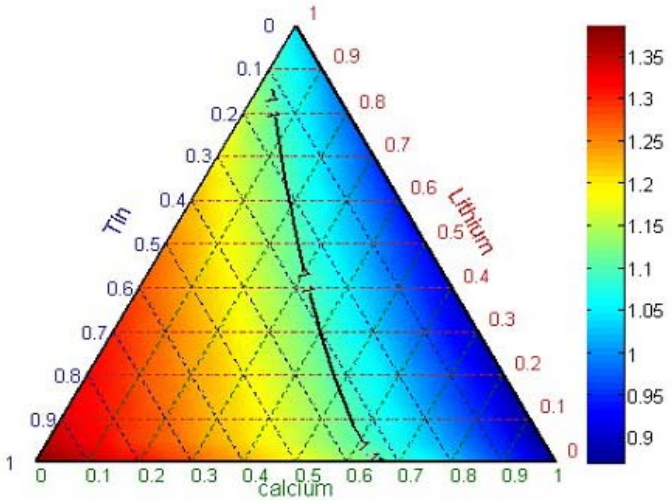

(b)

Figure 11: Tritium breeding ratio (a) and energy multiplication factor (b) for LiSnCa alloys as a function of composition.

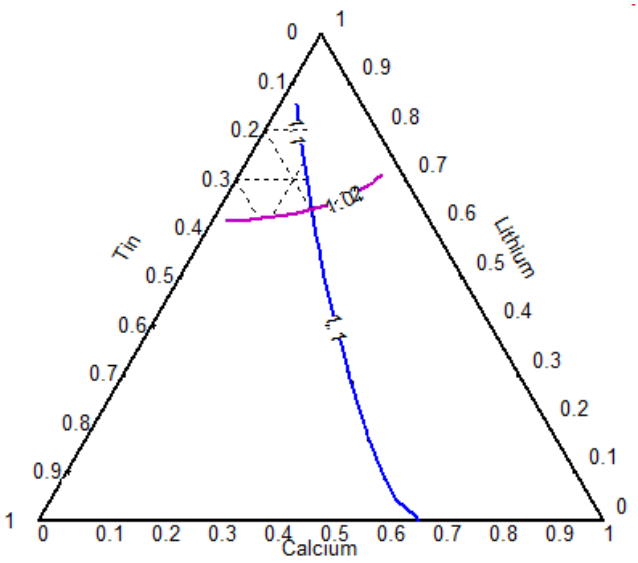

Figure 12: Acceptable domain of LiSnCa compositions.

Table 5: Properties of selected compositions within the acceptable domain for LiSnCa alloys.

Feature	Li, %	Sn, %	Ca, %	TBR	EMF
Min TBR, max EMF	61	37	2	1.02	1.21
Max TBR, min EMF	86	11	3	1.40	1.10
Reference	75	20	5	1.21	1.13
Min Li	61	37	2	1.02	1.21
Max Li	86	11	3	1.40	1.10
Max Sn	61	37	2	1.02	1.21

A composition of 75% lithium, 20% tin, and 5% calcium was chosen for further analysis. The flux spectra is very similar to that of the zinc mixture as show in Figure 13. The same dip due to lithium absorption is apparent. Similar to the previous case, the tritium reaction rate increases near the graphite reflector as seen in Figure 14. Figure 15 shows favorable tritium reaction rate in the thermal region, but larger energy deposited in the fast region.

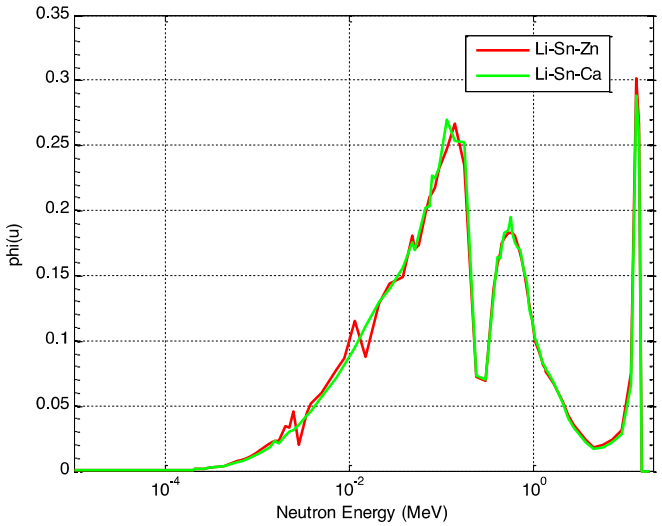

Figure 13: Neutron spectrum comparison of LiSnZn and LiSnCa.

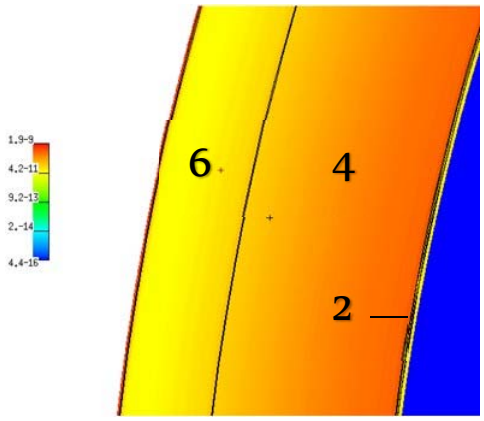

Figure 14: Spatial resolution of (n,t) reaction per unit volume the xz direction with blanket layers labeled (arbitrary scale).

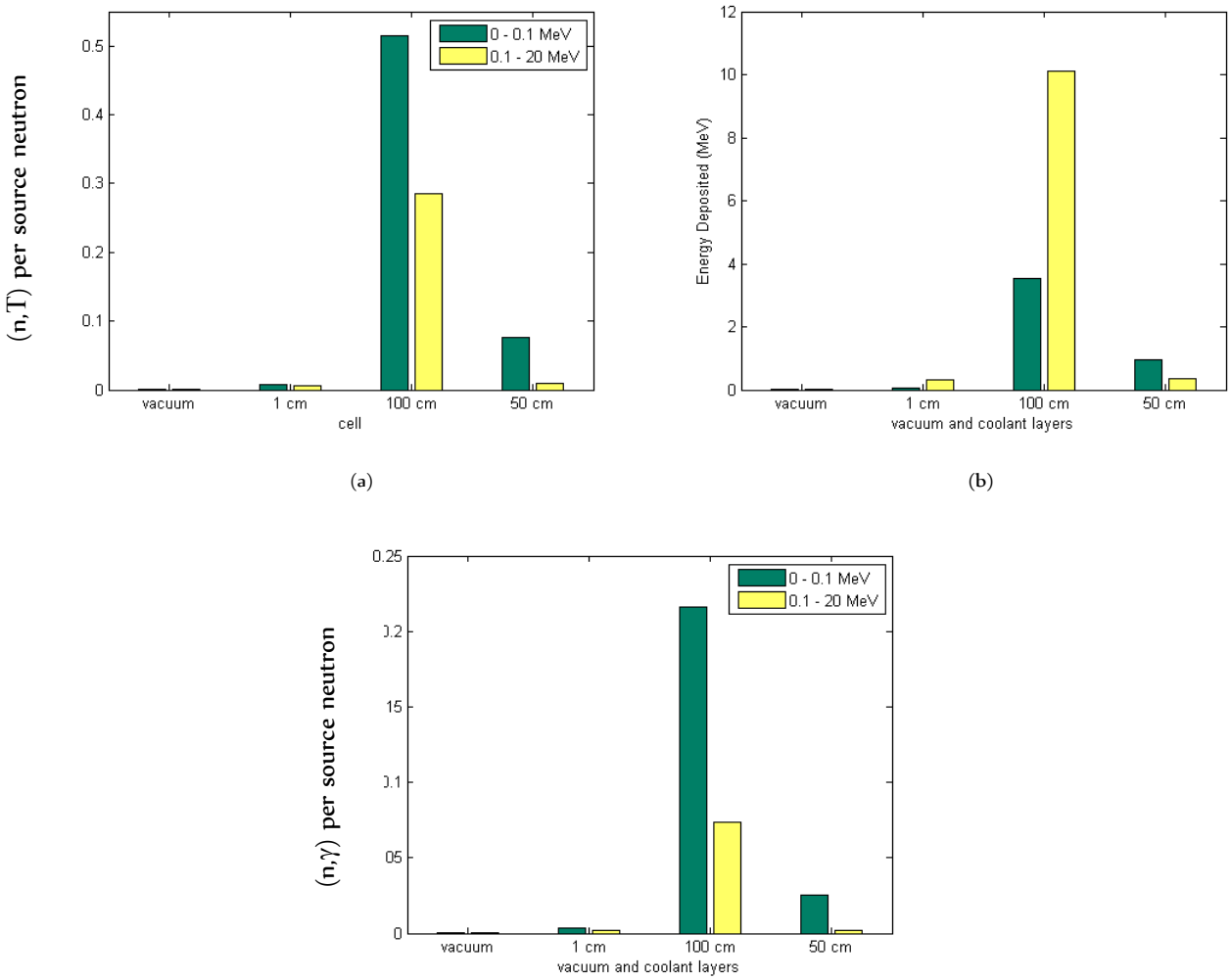

Figure 15: Comparison of thermal and fast spectra contributions for (a) tritium reactions, (b) total energy deposition and (c) gamma producing reactions for the alloy LiSnCa.

3.2.5 LiZnSb

Results for mixtures of lithium, zinc, and antimony are shown in Figure 16. These alloys have lower TBR and EMF than the lithium, tin, zinc alloys despite the higher Q-values for antimony; therefore, the area between TBR and EMF limits in Figure 17 is significantly smaller.

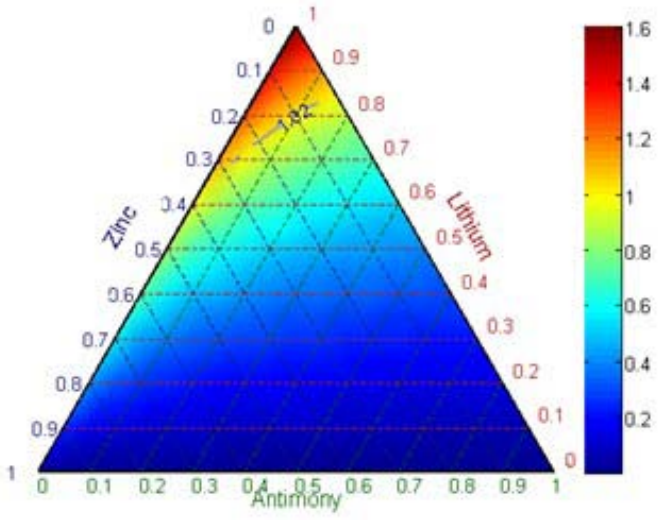

(a)

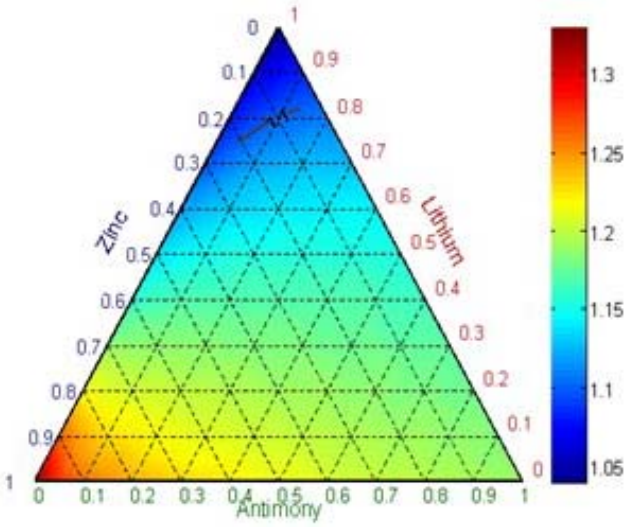

(b)

Figure 16: Tritium breeding ratio (a) and energy multiplication factor (b) for LiZnSb alloys as a function of composition.

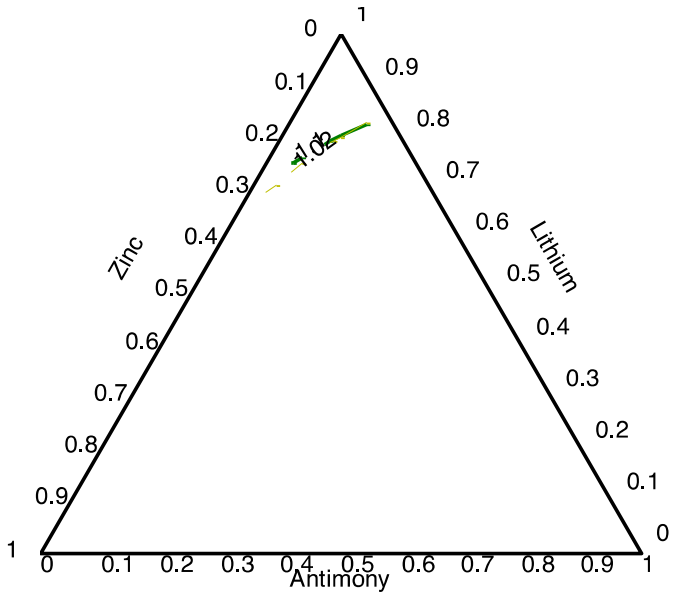

Figure 17: Acceptable domain of LiZnSb compositions.

3.2.7 LiZnGa

Results for mixtures of lithium, zinc, and gallium are shown in Figure 18. These alloys have lower TBR and EMF than the lithium, tin, zinc alloys despite the higher Q-values for gallium; therefore, the area between TBR and EMF limits in Figure 19 is also significantly smaller.

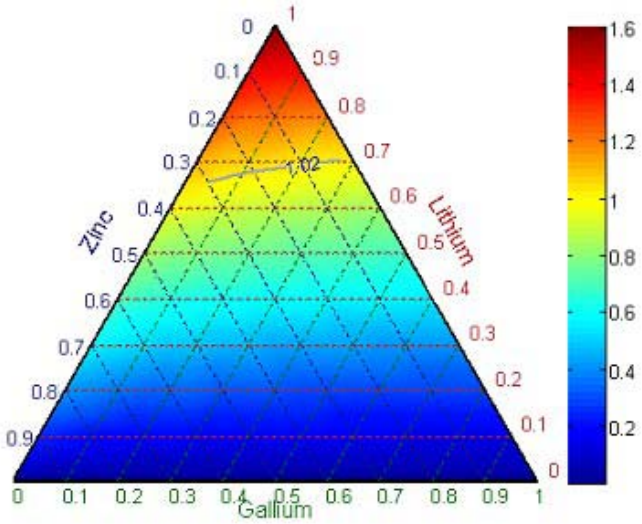

(a)

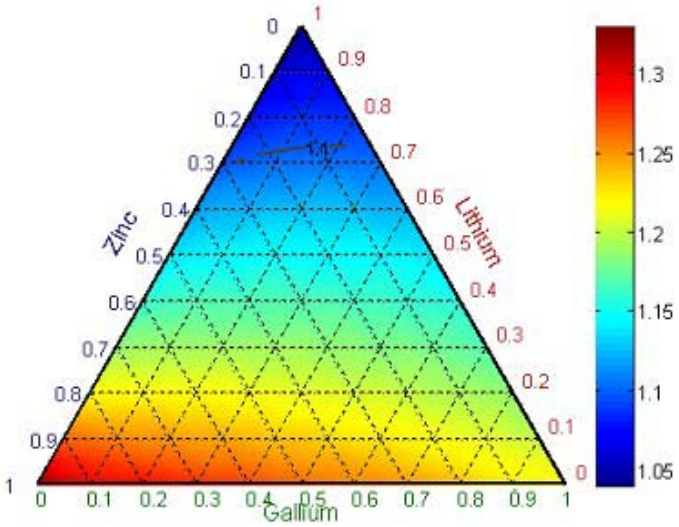

(b)

Figure 18: Tritium breeding ratio (a) and energy multiplication factor (b) for LiZnGa alloys as a function of composition.

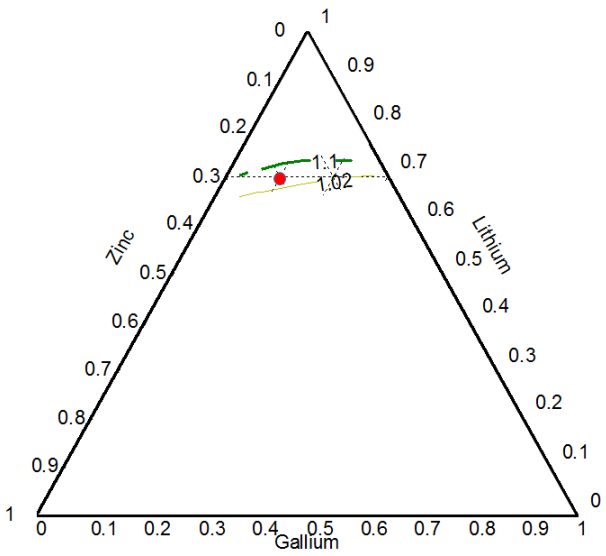

Figure 19: Acceptable domain of LiZnGa compositions.

3.2.9 LiPbSn

Results for the alloy composed of lithium, lead, and tin are illustrated in Figure 20. The range of lithium concentrations that have a TBR $\geq$ 1.02 and EMF $\geq$ 1.1 spans from 30% to 80%, Figure 21, much larger than any previous ternaries examined.

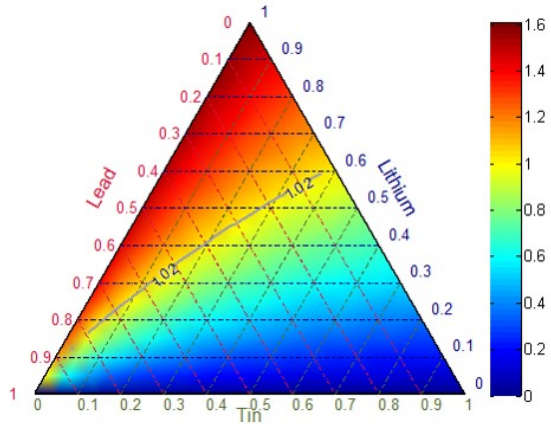

(a)

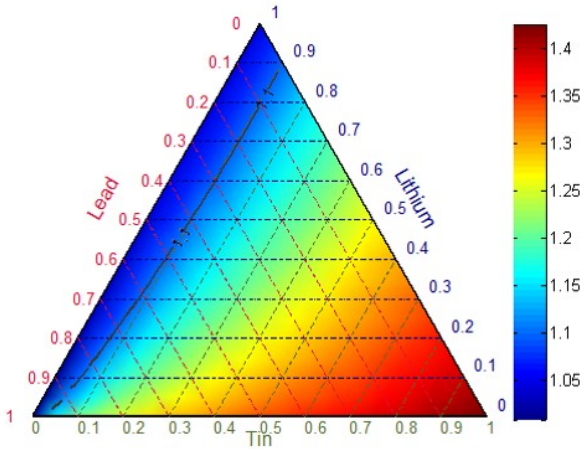

(b)

Figure 20: Tritium breeding ratio (a) and energy multiplication factor (b) for LiPbSn alloys as a function of composition.

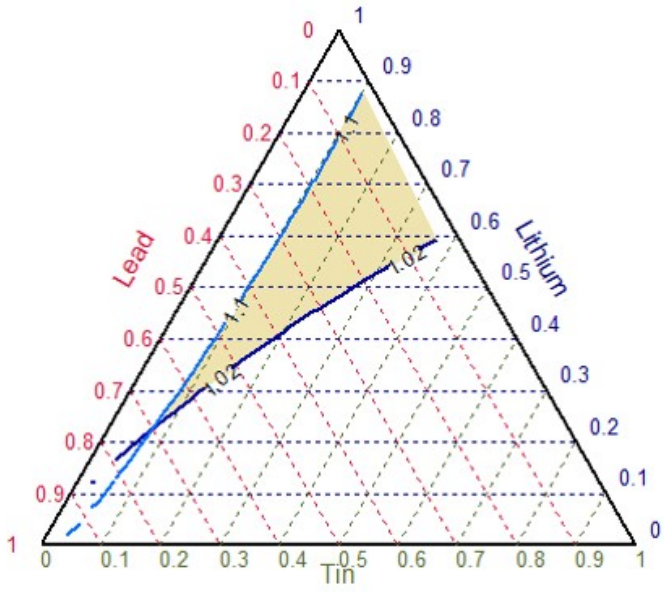

Figure 21: Acceptable domain of LiPbSn compositions.

3.2.11 LiSnBi

Results for the mixture composed of lithium, lead, and bismuth are illustrated in Figure 22. The composition domain that fits both the TBR and EMF minimum values is shown in Figure 23 and ranges between 30% and 80% lithium. This case is similar to LiPbSn; both mixtures contain tin, and the binary for bismuth has a similar trend to the binary of lead.

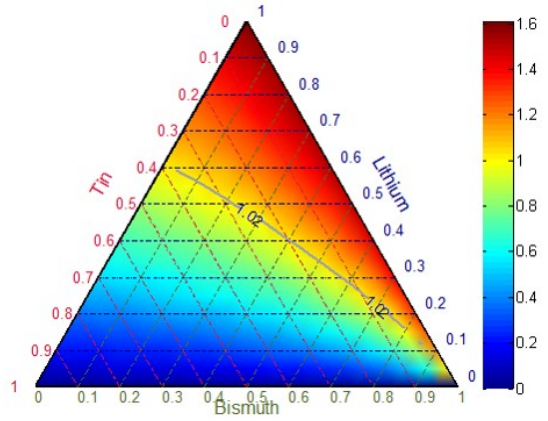

(a)

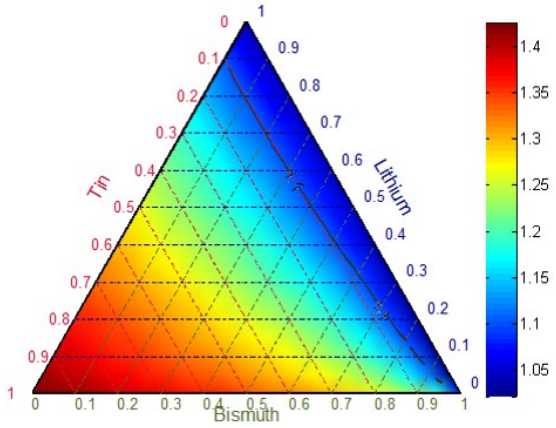

(b)

Figure 22: Tritium breeding ratio (a) and energy multiplication factor (b) for LiSnBi alloys as a function of composition.

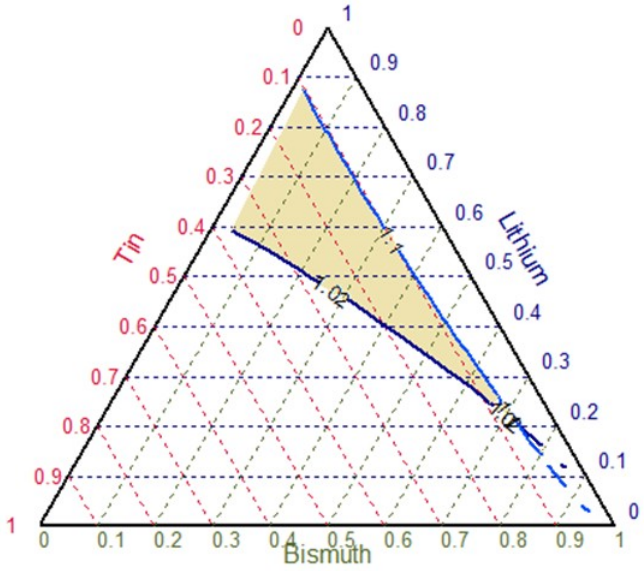

Figure 23: Acceptable domain of LiSnBi compositions.

3.2.13 LiBaBi

Figure 24 shows TBR and EMF results for LiBaBi alloys. The range of lithium concentrations that fit the TBR and EMF constrains, shown in Figure 25 is 20%-70%. When tin is swapped with barium the EMF increases at lower lithium concentrations, expanding across the majority bismuth compositions; the TBR is also higher at lower lithium and higher barium concentrations. As a result, the minimum and maximum lithium concentrations that meet the parameters decrease.

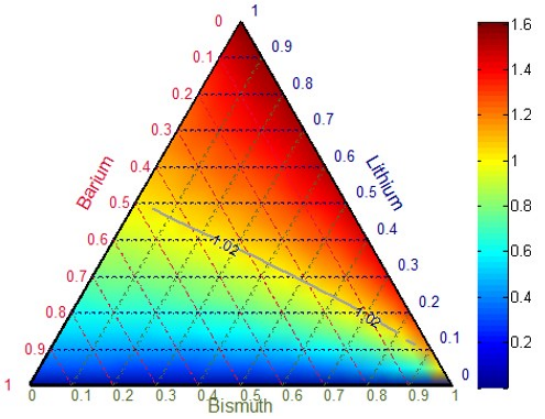

(a)

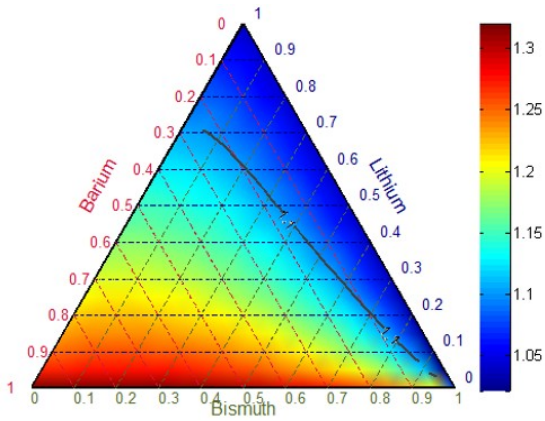

(b)

Figure 24: Tritium breeding ratio (a) and energy multiplication factor (b) for LiBaBi alloys as a function of composition.

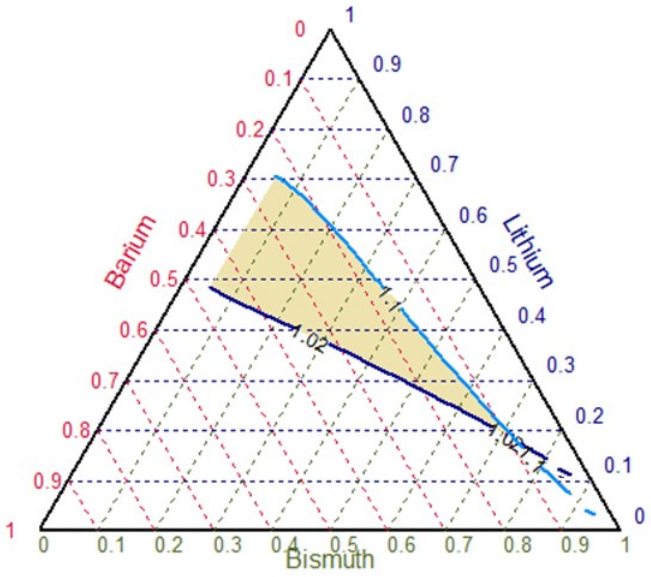

Figure 25: Acceptable domain of LiBaBi compositions.

3.2.15 LiPbBa

The results for the mixture consisting of lithium, lead, and barium are shown in Figure 26. The domain of lithium concentrations that achieves both minimum TBR and EMF is 25%-70%. This is only 5% less than the range for LiBaBi due to the similarities between bismuth and lead as seen in their binary plots.

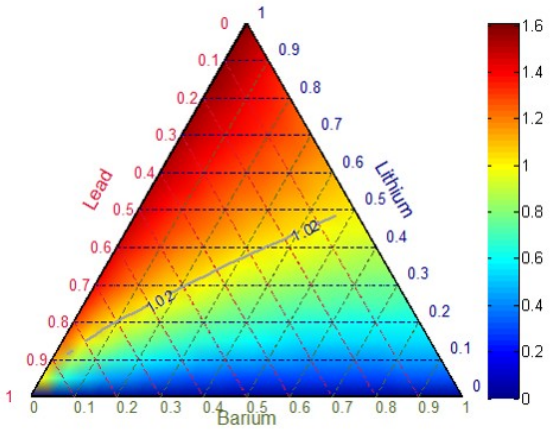

(a)

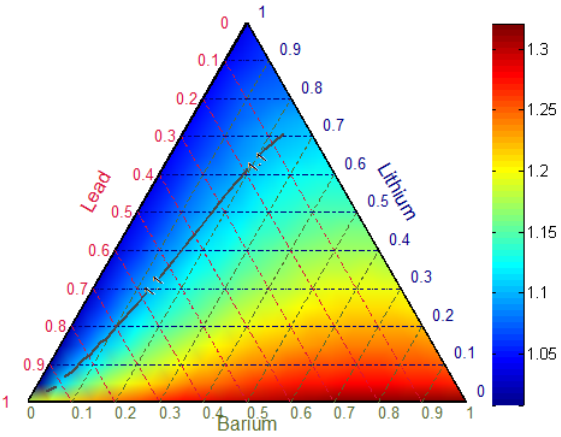

(b)

Figure 26: Tritium breeding ratio (a) and energy multiplication factor (b) for LiPbBa alloys as a function of composition.

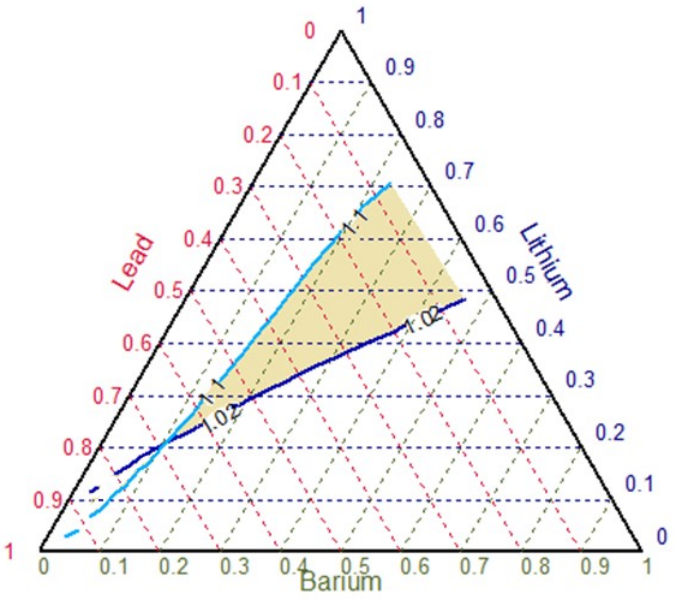

Figure 27: Acceptable domain of LiPbBa compositions.

3.2.17 *Additional Ternary Systems*

Acceptable composition domains are plotted for a variety of alloys in Figure 28.

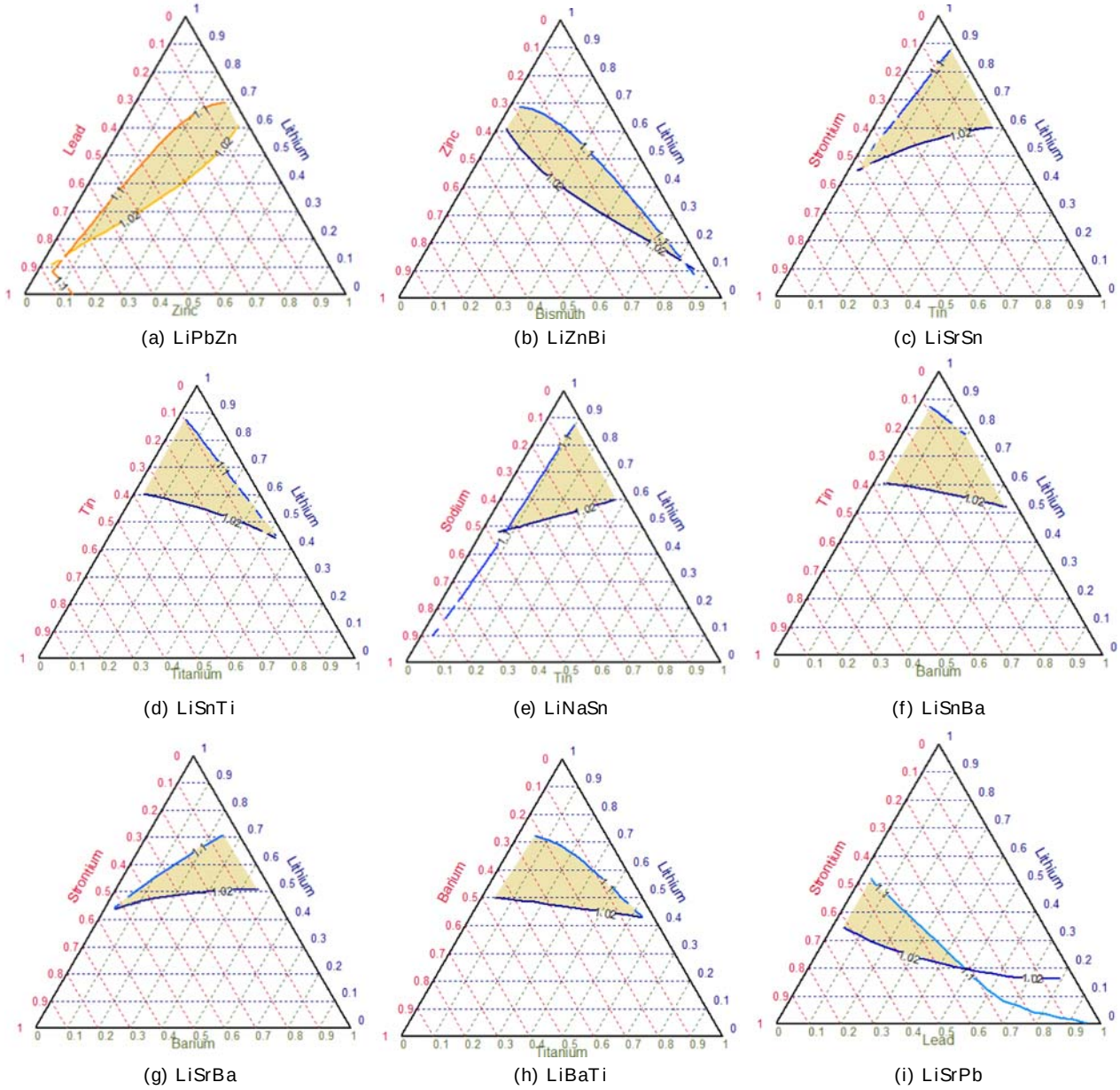

(a) LiPbZn (b) LiZnBi (c) LiSrSn

(d) LiSnTi (e) LiNaSn (f) LiSnBa

(g) LiSrBa (h) LiBaTi (i) LiSrPb

Figure 28: Acceptable domain of lithium ternary alloys.

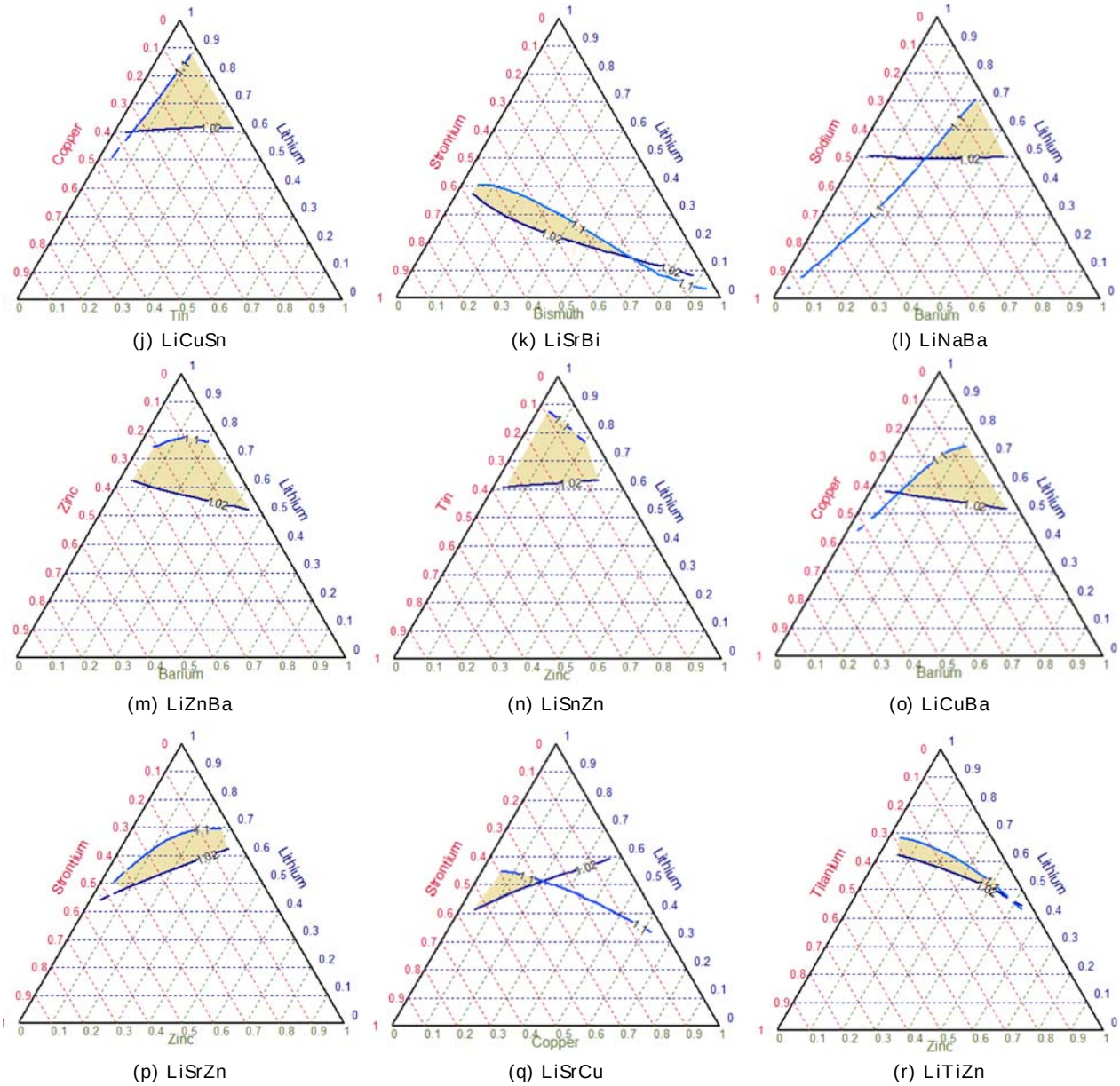

Figure 28: Acceptable domain of lithium ternary alloys.

3.4 DISCUSSION AND FUTURE WORK

The range of lithium concentrations within the acceptable TBR and EMF domain for each of the 34 alloys are listed in Table 6 in decreasing order and illustrated in Figure 29. Alloys containing Bi or Pb offer the wider range of acceptable compositions. Ternary alloys made of Li, Pb or Bi, and Zn or Sr or Ba can reduce lithium concentration below 25%. One important thing to note is the reactivity of the alkali and alkali earth metals in the period table, consisting of barium, strontium, and sodium. Avoiding these materials narrows down the best candidates to lead, bismuth, and tin. Additionally, if the EMF minimum was decreased to 1.0, all 34 elements would meet constrains, as outlined in Table 7 and Figure 30. Some elements that did not satisfy the requirements when the EMF limit was 1.1, such as LiCuBi and LiCuPb, become some of the choices when the EMF is lowered.

Future work will consider:

1. Continue the search for an optimal alloy formulation integrating the feedbacks from the thermodynamic study.
2. Evaluate options to improve blanket performance and extend the choice of acceptable alloys optimizing the blanket design.
3. Perform activation analysis of a subset of alloys to determine radiological hazard.
4. Perform sensitivity and uncertainty analysis of variables relevant to alloy development work and document.

Table 6: Range of lithium concentration in ternary alloys within acceptable domain when TBR $\geq$ 1.02 and EMF $\geq$ 1.1.

Alloy	Minimum Li, a%	Maximum Li, a%
LiPbSn	30	85
LiSnBi	30	85
LiBaBi	20	70
LiPbBa	25	70
LiPbZn	20	65
LiZnBi	20	65
LiSrSn	50	85
LiSnTi	50	85
LiNaSn	50	85
LiSnBa	55	85
LiSrBa	45	70
LiBaTi	45	70
LiSrPb	25	50
LiCuSn	65	85
LiSrBi	20	40
LiNaBa	50	70
LiZnBa	55	75
LiSnZn	65	85
LiCuBa	55	70
LiSrZn	50	65
LiSrCu	40	50
LiTiZn	55	65
LiNaZn	65	65
LiCuZn	65	65
LiSrTi	45	45
LiNaTi	0	0
LiPbBi	0	0
LiCuBi	0	0
LiNaPb	0	0
LiNaBi	0	0
LiTiBi	0	0
LiNaSr	0	0
LiCuPb	0	0
LiNaCu	0	0

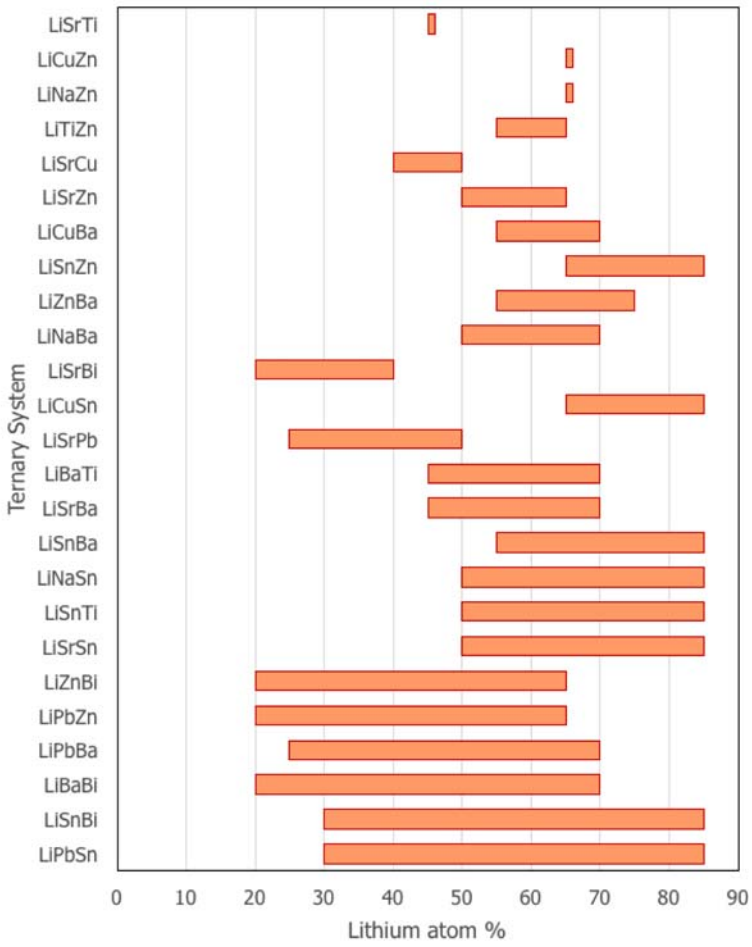

Figure 29: Summary of lithium ranges for ternaries that meet TBR $\geq$ 1.02 and EMF $\geq$ 1.1 constraints.

Table 7: Range of lithium concentrations in ternary alloys within acceptable domain when TBR $\geq$ 1.02 and EMF $\geq$ 1.0.

Alloy	Minimum Li, a%	Maximum Li, a%
LiNaPb	5	95
LiNaBi	5	95
LiPbBa	10	95
LiPbBi	10	95
LiCuBi	10	95
LiSrBi	10	95
LiPbZn	10	95
LiTiBi	10	95
LiCuPb	10	95
LiSnBi	10	95
LiBaBi	10	95
LiZnBi	10	95
LiPbSn	10	90
LiSrPb	20	95
LiSrCu	40	95
LiNaTi	45	95
LiSrSn	45	95
LiSnTi	45	95
LiSrBa	45	95
LiBaTi	45	95
LiNaSr	45	95
LiTiZn	45	95
LiSrZn	45	95
LiSrTi	45	95
LiNaBa	50	95
LiNaSn	50	95
LiNaCu	50	95
LiCuBa	55	95
LiZnBa	55	95
LiNaZn	55	95
LiSnBa	55	95
LiCuSn	60	95
LiCuZn	60	95
LiSnZn	65	95

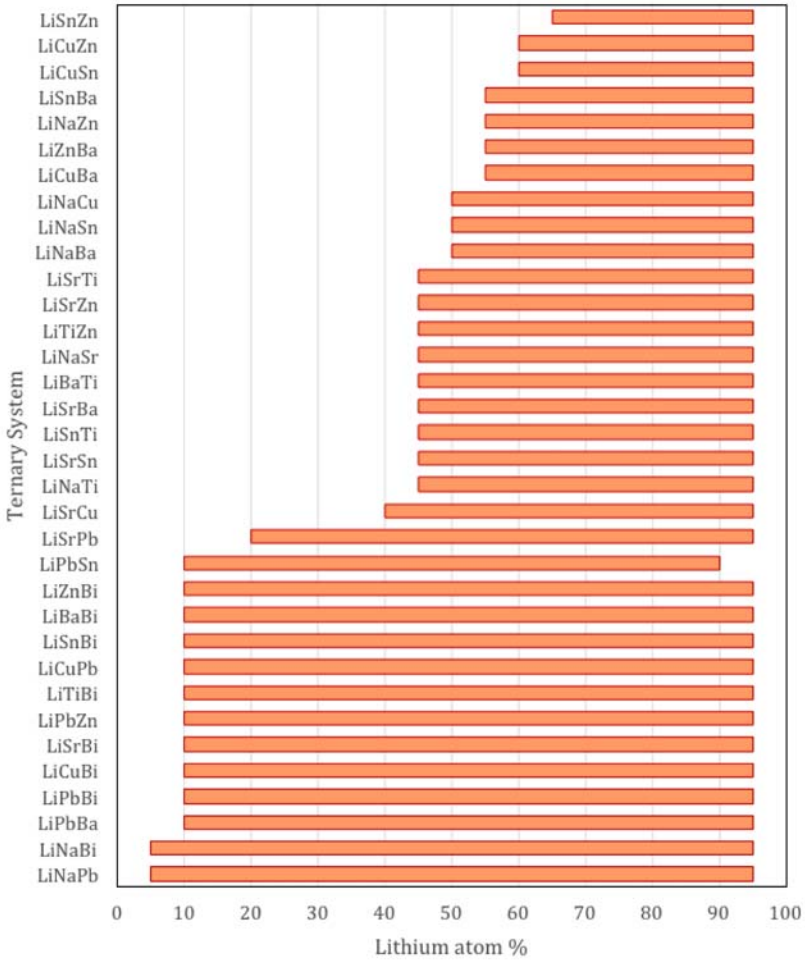

Figure 30: Summary of lithium ranges for ternaries that meet TBR constraint and EMF of 1.0.